ADSORPTION KINETICS AND THERMODYNAMICS OF CIPROFLOXACIN FROM AQUEOUS SOLUTIONS BY MAGNETIC IRON OXIDE NANOPARTICLES MODIFIED *MORINGA* PODS

Mokete John Phele[1, 2], Fanyana Moses Mtunzi[1, 2], Joe Modise[2], David Shooto[2]

[1]Department of Chemistry, Faculty of Applied and Computer Sciences, Vaal University of Technology, Vanderbijlpark, 1911, South Africa, phelemj85@gmail.com
[2]Institute of Chemical and Biotechnology, Faculty of Applied and Computer Sciences, Vaal University of Technology Southern Gauteng Science and Technology Park, Sebokeng, 1983, South Africa

ORIGINAL SCIENTIFIC PAPER

ISSN 2637-2150
e-ISSN 2637-2614
UDC 612.014.46:546.562-31
DOI 10.7251/STEDZ2402010P
COBISS.RS-ID 141779201

Received: *21 October 2024.*
Accepted: *11 November 2024.*
Published: *29 November 2024.*
http://stedj-univerzitetpim.com

Corresponding Author:
Mokete John Phele, Department of Chemistry, Faculty of Applied and Computer Sciences, Vaal University of Technology, Vanderbijlpark, 1911, South Africa, phelemj85@gmail.com

Citation:
Phele, M.J., Moses Mtunzi, F., Modise, J., & Shooto, D. (2024). Adsorption vinetics and thermodynamics of ciprofloxacin from aqueous solutions by magnetic iron oxide nanoparticles modified *Moringa* pods. *STED Journal*, *6*(2), 10-24.

ABSTRACT

The adsorption process of metal oxide nanoparticles has been studied as an effective means of removing organic and inorganic contaminants from water and wastewater. In this study, iron (III) oxide (Fe_3O_4) nanoparticles were synthesized in the presence of *moringa oleifera* pods (MOP) as an adsorbent for ciprofloxacin (CIP) adsorption. *Moringa oleifera* pod biochar with Fe_3O_4 particles precipitated on the surface of biochar was synthesized by co-precipitation method. The effect of various parameters such as contact time, pH, metal concentration and adsorbent dosage on the removal efficiency was determined. The maximum adsorption capacity of CIP by magnetic *moringa* composite (MMC) was 96.12 mg/g. The Langmuir and Freundlich isotherm equations were used to analyze the equilibrium isotherm data. The adsorption process fit well with the second-order kinetics in all cases, and the Langmuir isotherm equation fitted well with the experimental data.

Keywords: *Moringa Oleifera*, Iron oxide, Ciprofloxacin, Nanoparticles.

INTRODUCTION

Water from rivers and lakes is crucial for life to continue. The way it's utilized and discarded is a global environmental problem (Gleick, 2003). In particular, due to the high susceptibility to pollution of water bodies (Mushtaq, Singh, Bhat, Dervash, & Hameed, 2020), which can be polluted by different sources such as microbial, chemical, physical or biotic factors (World Health Organization [WHO], 2017). The main cause of water pollution is anthropogenic activities and the rapid increase in human population is making the situation worse (Gleick, 2003).

Overcrowded areas, industrial activities, chemicals, debris, hospital sewage contaminated with antibiotics, etc. are just a few examples of the damage done to the planet's water sources (Mushtaq, et al., 2020). There are numerous worries regarding the use of antibiotics, such as ciprofloxacin (CIP), in both surface and drinking water, as they may present a risk to both the environment and human well-being. Long-term toxicity, hormonal interference, and direct harm to microorganisms, even in small amounts, are among these issues. (Yahya, et al., 2014). Ciprofloxacin is a clinically used third-generation fluoroquinolone with potent, broad-spectrum antibacterial activity. Recent research has reported a large number of emerging pollutants whose metabolites have been identified in aqueous media. A number of promising wastewater treatment methods have been used to remove CIP from wastewater, such as: B. membrane separation (Avella, et al., 2010), ozonation (Witte, et al., 2010), Naofiltration (Sun, Hatton, & Chung, 2011), photocatalytic degradation (Van Doorslaer, Demeestere, Heynderickx, Van Langenhove, & Dewulf, 2011), and adsorption (Carabineiro, Thavorn-Amornsri, Pereira, Serp, & Figueiredo, 2012). One of them, adsorption, is considered a promising method for removing CIP (Zhang, Qiao, Zhao, & Wang, 2011), from wastewater in terms of its simple construction, easy operation, large surface areas, developed porous structures, rich functional groups, and high and low adsorption capacity. Various adsorbents including activated carbon, chitosan-metal microparticles (Reynaud, et al., 2011), coal fly ash (Zhang, et al., 2011), kaolinite (Li, et al., 2011), and dioctahedral clay minerals (Wang, Li, & Jiang, 2011).

In this study, the Fe_3O_4 magnetic nanoparticles modified with *Moringa oleifera* pods were prepared using the chemical co-precipitation method. The influences of pH, adsorbent dose, and contact time, CIP initial concentration, and solution temperature on the adsorption capacity were investigated. The adsorption kinetics and thermodynamics were also examined.

EXPERIMENTAL

Material and Methods

Collection and Preparation of *Moringa Oleifera* Pods

Moringa oleifera pods were collected from trees in Limpopo farm near Polokwane. Soon after collection, pods were washed thoroughly with doubly distilled deionized water to remove water soluble impurities and oven dried at 105°C for 24 hours. The washed and dried material was pulverized (by mortar and pestle) and sieved to different mesh sizes. The sieved material was rewashed thoroughly with doubly distilled deionized water to remove the fine particles and dried at 105°C for 4 hours. The material was treated with 0.1M nitric acid and methanol for 4 hours to remove inorganic and organic matter from the sorbent surface and dried in an electric furnace. The treated and untreated materials were then placed in a desiccator to be used as sorbents.

Batch biosorption experiments were conducted to investigate the influence of physiochemical parameters such as contact time, initial concentration, adsorbent dosage, and temperature on CIP adsorption. Batch experiments were performed for different CIP concentrations (10 - 60 mg/L), temperature (14 - 50°C), adsorbent dose (0.1- 0.6 g/L) and contact time (0 - 180 min). After prescribed contact time, the solution was filtrated using filter syringe and the concentration of CIP in the filtrate was measured using UV-Vis.

Preparation of the iron oxide magnetic nanoparticles, biochar, and composite

The Fe_3O_4 magnetic nanoparticles (MNP) were prepared from a 400mL solution of $FeCl_3$ (7.8 g, 28 mmol) and $FeSO_4$ (3.9 g, 14 mmol) at room temperature using the chemical co-precipitation method (Oliveira, et al., 2003). The solution was continuously stirred with an overhead stirrer while 1.0M NaOH solution was added dropwise to precipitate the MNP. The MNP was magnetically separated, washed with water and then ethanol before drying. The mass of MNP after drying was noted.

The pulverized *moringa* pods (PMP) was separately charred in a crucible at 250°C for 4 hours to obtain the *moringa* biochar (MBC).

The biomass was first dried at 110°C for 1 hour before increasing the temperature at a rate of 5°C.min^{-1} until 250°C which was maintained for 4 hours. The PBC was then cooled, ground, sieved through a 230 mm mesh size sieve. This was followed by washing until the filtrate was colourless indicating no leaching of residual Fe or carbon. The MBC was again dried at 105°C for 2 hours, cooled, weighed noted, and stored.

The MBC-MNP combo (MMC) was prepared by calcining the treated *moringa* pods (MOP) and MNP. The MNP was prepared by chemical co-precipitation in the presence of the treated MOP and subsequently calcined at 250°C. Typically, the MOP was suspended in a 400 mL solution of $FeCl_3$ (7.8 g) and $FeSO_4$ (3.9 g) and stirred thoroughly to allow for wetness. A solution of 1.0M NaOH solution was added dropwise to raise suspension pH to 10 and precipitate the MNP on the MOP surface. The solution was further stirred for 30 min before separation by centrifugation at 2500 rpm for 4 min. followed by filling of the residue into a crucible for the calcining process. The crucible was heated at 110°C for 1 hour before raising the temperature at a rate of 5°C/min until 250°C which stood for 4 hours. After the calcining process, the MMC combo was cooled and washed with water until the filtrate was colourless indicating no leaching of organic matter or iron. The MMC was subsequently dried at 105°C for 2 hours and stored.

Data Management.

Adsorption capacity (mg. g^{-1}) at equilibrium for adsorption of analyte were determined by equation 1.

$$q_e = \frac{(C_0 - C_e)}{M} V \qquad (1)$$

where Co and Ce are the initial and final pollutant concentrations (mg/L), respectively, while M (mg) and V (mL) are the MMC mass and solution volume, respectively.

Adsorption Isotherm of MMC

Langmuir and Freundlich adsorption isotherm models were used to depict the equilibrium between adsorbed CIP on MMC (q_e) and CIP concentration in solution (C_e) at constant temperature (30 °C).

Kinetic Study of MMC

The pseudo-first order and pseudo-second order kinetic models were used to describe the adsorption process.

Thermodynamic Parameters

Thermodynamic parameters such as Gibbs free energy (ΔG), enthalpy (ΔH) and entropy (ΔS) for the adsorption of cations on MMC are calculated using the following equations (Machado, Lazarin, & Airoldi, 2006; Guerra, Lemos, Airoldi, & Angelica, 2006):

$$\Delta G = -RT\, InK_L$$

where K_L is the equilibrium constant obtained from Langmuir model, T the absolute temperature (K) and the universal gas constant R=8.314×10^{-3} kJK^{-1}mol^{-1}. The relationship between K_L and thermodynamic parameters of ΔH and ΔS can be described by the Van't Hoff correlation in the following equation (Celik, & Ozdemir, 2018; Yildiz, Erol, Aktas, & Alimli, 2004):

$$InK_L = \frac{\Delta S}{R} - \frac{\Delta H}{RT}$$

The thermodynamic study was made at three different levels of temperatures which were 298, 313 and 343 K.

Sample preparation for FTIR analysis

An approximately amount of 150 mg of potassium bromide (KBr) was mixed with about 1 mg of the sample. The mixture was crushed using pestle and mortar, thereafter a small amount of the crushed fine powder was loaded into three pieces of the pellet press using spatula. The three pieces of the pellet press was transferred to hydraulic press for compression for about 2 minutes. The resulted pellets were introduced into FTIR instrument for analysis. The experimental condition for

FTIR analysis (Bruker-Alpha, Germany), the scan range was 400 – 4500 cm^{-1}.

Scanning Electron Microscope (SEM)

Scanning electron microscopy (SEM) was used to observe the microstructure and surface morphology of MOP and MMC. The SEM images were obtained on a Cerl-Zeiss Sigma instrument (Germany) that uses a tungsten filament source. The samples were Pd-Au coated and imaging was done at 5 kV.

Thermogravimetric Analyser (TGA)

The TGA normally require no sample preparation. In this study an approximately amount of 10 mg of the sample was loaded into TGA ceramic crucible and introduced to TGA instrument for analysis. Table 1 below shows experimental conditions for TGA analysis.

Table 1: Experimental set up conditions for TGA analysis.

Instrument's name	**Hitachi-STA7200RV, Japan**
Parameters	
Temperature range	30-650 °C
Nitrogen flow	20 ml/min
Heating rate	10 °C/min
Holding time	3 min

RESULTS AND DISCUSSION

Fourier transform infrared spectrometry (FTIR)

The main functional groups responsible for adsorption present in the magnetic iron oxide nanoparticles modified with *Moringa oleifera* pods, were characterized by infrared analysis. The FTIR spectra were recorded in transmittance band mode in the wavelength range from 4400 cm^{-1} to 400 cm^{-1} as shown in Figures 1 and 2.

Using FTIR, it's possible to verify whether various pollutants can effectively be adsorbed onto MOP, achieving both adequate and satisfactory removal rates. As shown in Figures 1 and 2, the FTIR spectroscopic analysis indicated band at 3326 cm^{-1}, representing bonded – OH groups.

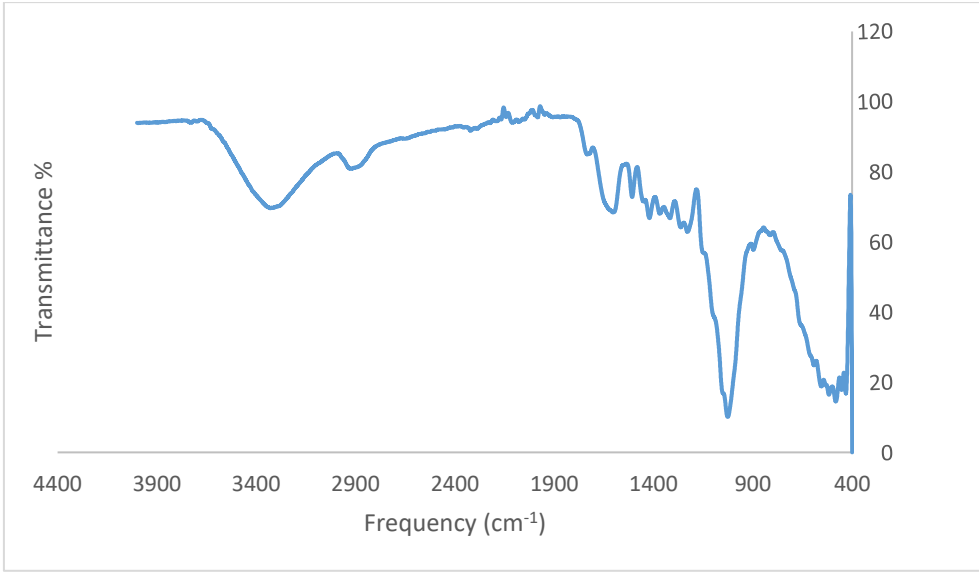

Figure 1. FTIR spectrum of *moringa oleifera* pods.

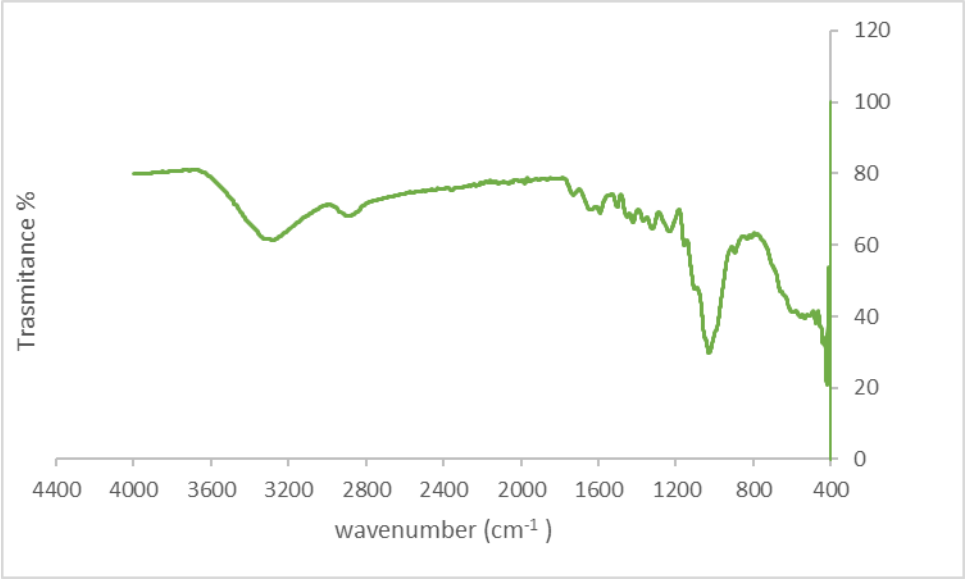

Figure 2. FTIR spectrum of magnetic *moringa oleifera* pods.

The band observed at 2917–2849 cm^{-1} was assigned to the aliphatic C–H group. The peak around 1623 cm^{-1} corresponds to C=O stretch. The peak observed at 1541 cm^{-1} corresponds to the secondary amine group, while the peak at 1374 cm^{-1} corresponds to the symmetric bending of CH_3; the one observed at 1314 cm^{-1} corresponds to the C–H bending. Also, the peak observed at 1242 cm^{-1} corresponds to the $–SO_3$ stretching, at 1029 cm^{-1} corresponds to C=O bonds of ether, ester or phenol, at 668 cm^{-1} corresponds to –CN stretching, while the peak observed at 564 cm^{-1} corresponds to S–O. On the other hand, typical functional groups for iron oxide are depicted by absorption band at 3660 cm^{-1} that corresponds to the hydroxyl functional group and a band obtained at 531 cm^{-1} is characteristic of $M_{tetrahedral}$ resonance with O (Kandpal, Sah, Loshali, Joshi, & Prasad, 2014). This peak also relates to Fe-O group.

Scanning Electron Microscope (SEM)

The SEM images (Figures 3(a-b)) were evaluated to study the surface morphology of the adsorbents prior to adsorption of CIP. The SEM images of the MOP biomass were inherently foamy and fibrous with no particular shape as reported elsewhere (Tavengwa, Cukrowska, & Chimuka, 2016). However, after thermal treatment (250°C), the surface morphology showed macropores and irregular trough-like patterns. The structure appeared weak and the cell morphology of the vegetable biochar was absent. The micrographs of MOP (Figure 3(a)) shows mesoporous structures with different pore sizes. These surface properties would result in high CIP binding due to the available binding voids for the CIP. The porosity for the magnetic *Moringa* composite has improved compared to the modified MOP. Therefore, this can explain the difference in the adsorption capacity of CIP using these adsorbents. As also shown, the magnetite composite appears to be agglomerated, which could be attributed to strong binding of nanoparticles, magnetic dipoles as well as van der Wall forces (Ehrampoush, Miria, Salmani, & Mahvi, 2015). Under these circumstances, one can deduce that dispersing the adsorbent particles before using them in the adsorption process is a necessary step to take full advantage of the particle surface area (Nasseh, Al-Musawi, Miri, Rodriguez-Couto, & Hossein-Panahi, 2020).

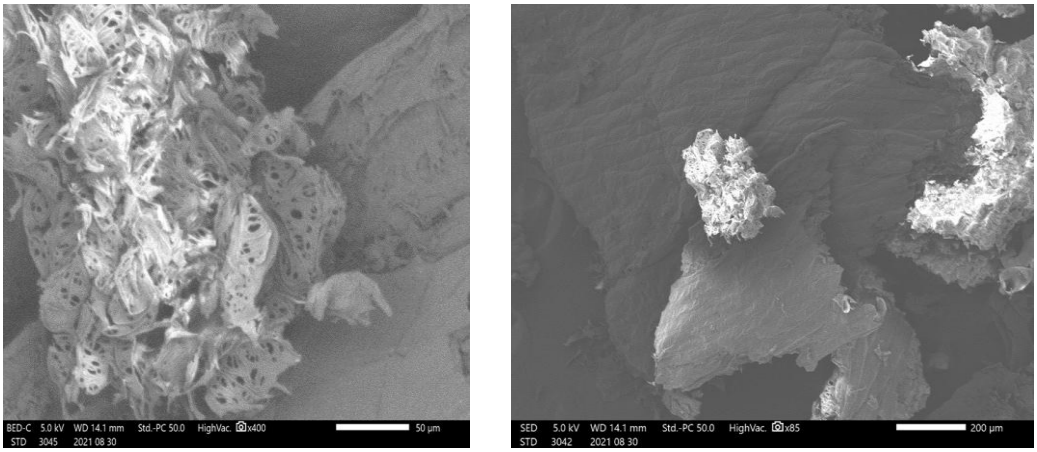

Figure 3. SEM images: (a). MOP before adsorption, (b). MMC before adsorption

Thermogravimetric Analyser (TGA)

The thermal stability of MMC was examined when MMC was heated from 20.5°C to 800°C as shown in Figure 4. The various thermal decomposition states in terms of percent weight loss and their respective derived weight loss percentages per C were reported by Araujo, et al., (2010). The first stage between 20°C and 100°C involves water loss, or the water desorption process occurs during the initial phase of decomposition. The second stage between 100 °C and 350 °C could be due to the loss of organic matter, which could contain amino acid residues from proteins with different functional groups and other low molecular weight compounds. The third stage between 350°C and 780°C could consist of higher boiling point compounds. At the end of the decomposition stage (780° C), the total residue was thus reached.

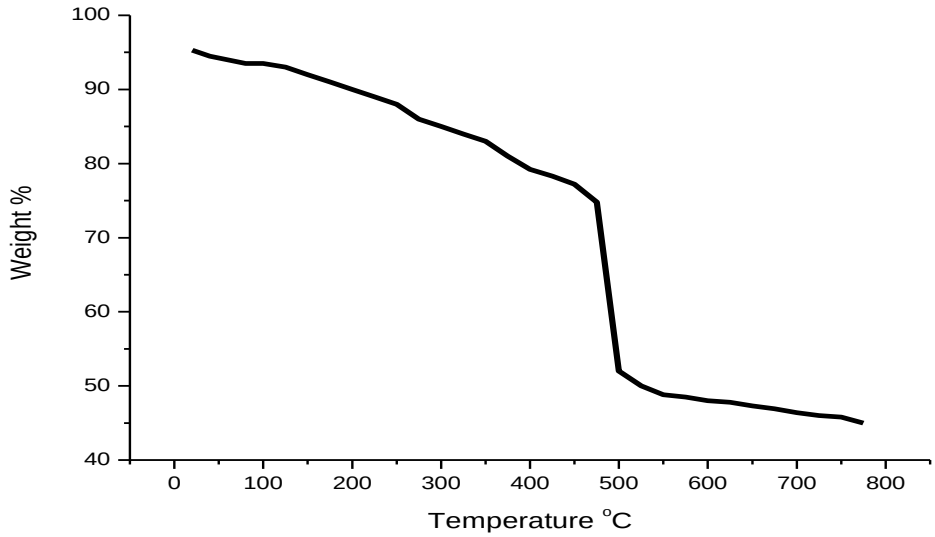

Figure 4. TGA curve for MMC

Effect of biosorbent dose

The influence of the adsorbent dose (0.1-0.6 g/L) at an initial CIP concentration of 10 mg/L was tested at 30°C. As shown in Figure 5, the results show that the CIP removal rate increased sharply with increasing adsorbent dose (from 0.1 to 0.2 g/L) and then more slowly from 0.2 to 0.6 g/L increased. This result may be due to the increase in the number of adsorption sites and the increase in surface area with increasing amount of adsorbent. Therefore, 0.3 g/L of the adsorbent dose was used in subsequent experiments.

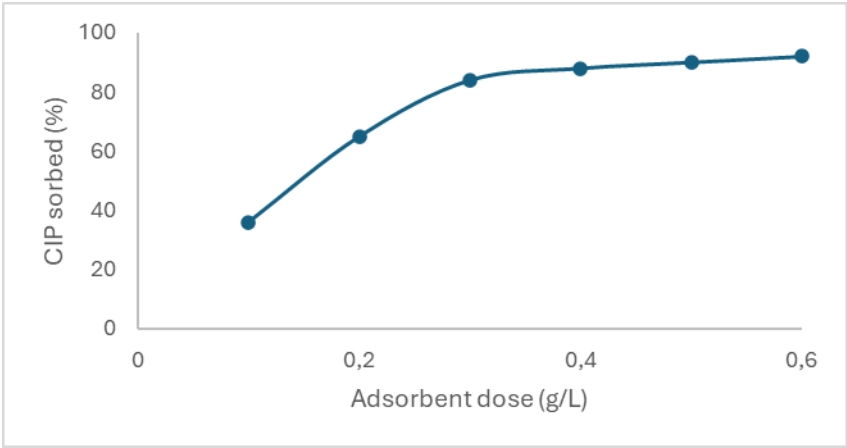

Figure 5. Effect of adsorbent dose for the adsorbent on adsorption removal

Effect of contact time

The effect of contact time is one of the important parameters that helps determine the equilibration time as well as provide insight into the sorption rate and mechanism. The results obtained, Figure 6, showed that the adsorption rate was high during the first 60 minutes, reaching about 85% of the total CIP sorbed by MMC. After 60 min the sorption rate was relatively slow, there were numerous available active sites on the adsorbent surface. As the sites were occupied, the rate of adsorption gradually decreased (Kakavandi, Esrafily, Mohseni-Bandpi, Jafari, & Kalantary, 2013). Adsorption reached equilibrium at 120 min for MMC. A contact time of 180 minutes was therefore chosen for further tests.

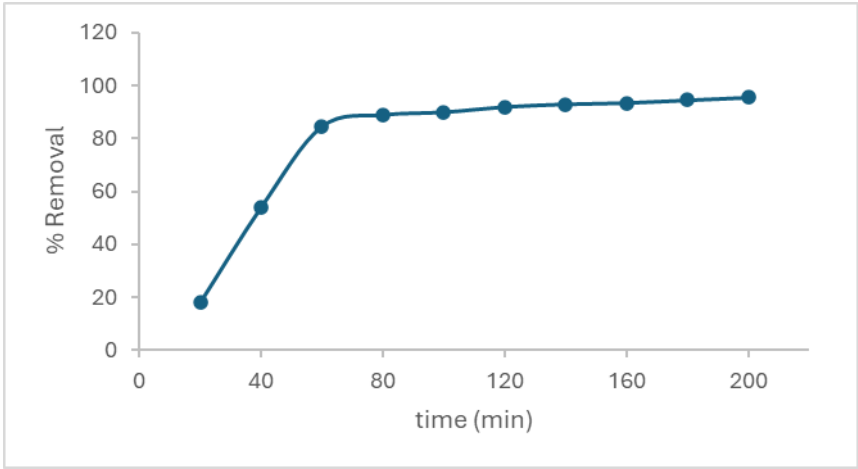

Figure 6. Effect of contact time on CIP removal

Effect of pH

In a broader context, the pH level of a solution is regarded as a significantly impactful variable that determines the adsorption process. It has been found that pH affects the surface charge of the adsorbent, Figure 6 shows the effect of pH on CIP adsorption. The results show a higher rate of CIP adsorption removal in the range of pH 6-9. For CIP, the acid dissociation constants are 6.1 for the carboxylic acid group (pK_{a1}) and 8.7 for the basic N-unit (pK_{a2}) (Gu, & Karthikeyan, 2005). Therefore, CIP molecules exist mainly as cations at pH < 6.1 due to protonation of the amine group. At pH > 8.7, CIP molecules exist as anions due to deprotonation of carboxylate. At a pH in the range of 6.1 to 8.7, CIP molecules exist as zwitterions. In addition, the PZC of the adsorbent is pH 7.3. Therefore, if the solution has a pH < 7.3, the adsorbent surface will be positively charged; however, at pH > 7.3 the adsorbent surface becomes negatively charged. Accordingly, the electrostatic interaction between charged CIP molecules and the charged adsorbent surface at pH < 6 and pH > 9 (Figure 7) is optimal conditions for the adsorption process. At pH in the range of 6-9, the CIP molecules and the adsorbent surface have opposite charges, resulting in a high removal rate of adsorption pH < 6 and pH > 9.

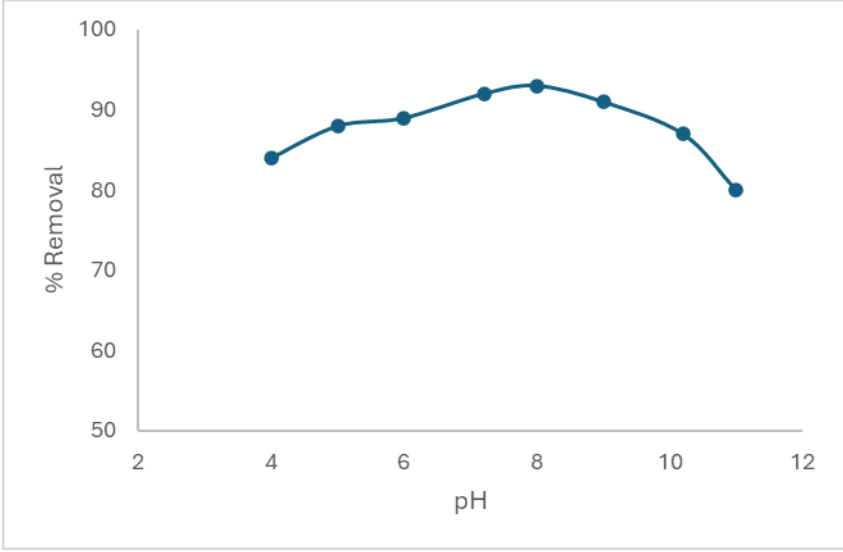

Figure 7. Effect of pH for the adsorbent on adsorption removal

Initial metal concentration

The initial concentration provides a significant driving force to overcome the total mass transfer resistance of CIP between the aqueous and solid sorbent. The effect of the initial CIP concentration is shown in Figure 8. CIP adsorption capacity increased with increasing initial CIP concentration. Figure 8 also shows that the rate of CIP removal decreased as the initial concentration increased from 10 to 60 mg/L. This may be due to the limitation of available free space on MMC for CIP adsorption.

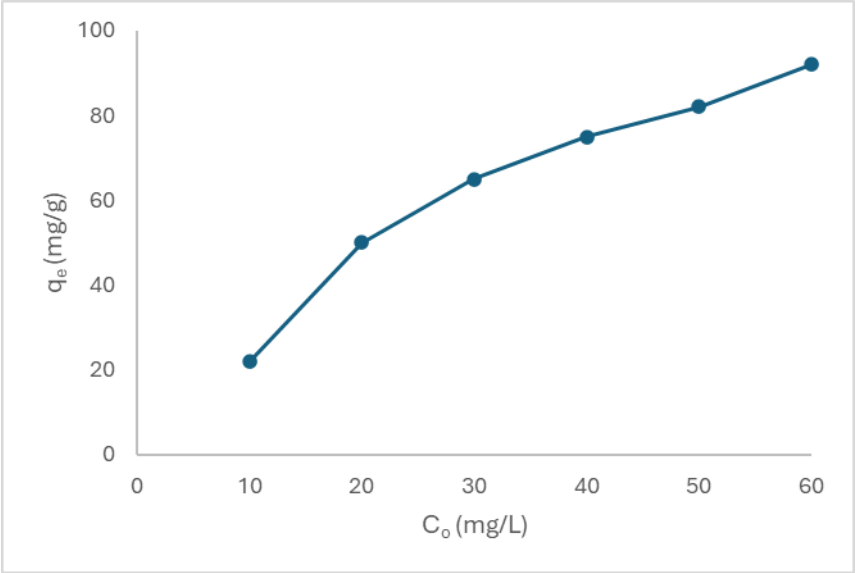

Figure 8. Effect of initial CIP concentration for MMC on adsorption capacity

Effect of temperature

The effect of temperature on CIP adsorption is shown in Figure 9. As shown in the figure, the adsorption capacity increased with increasing temperature, indicating that the adsorption is endothermic. This trend shows that increasing the temperature is beneficial for adsorption. Increasing the temperature increases the mobility of CIP towards the sorbent and can also cause a swelling effect within the internal structure of the sorbent and therefore allow the CIP to penetrate further or increase the surface area for CIP to bind.

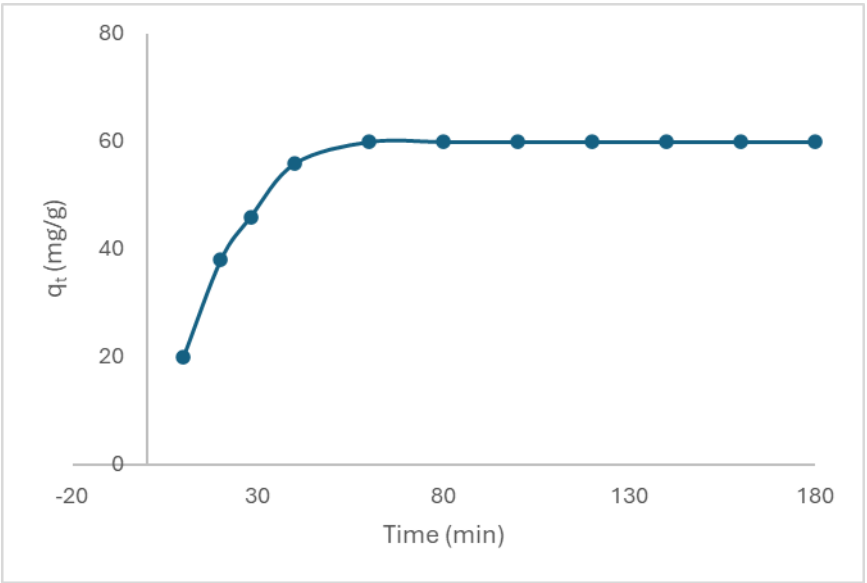

Figure 9. The effect of temperatures on adsorption capacity

Adsorption isotherms

The adsorption isotherms were fitted by the Langmuir and Freundlich models. Table 2 shows the obtained sorption isotherm constants for magnetic *Moringa* biosorbent according to the Langmuir and Freundlich models. We can observe that the Langmuir model is more suitable for describing the adsorption process than the Freundlich model. Therefore, we can assume that the CIP adsorption occurs mainly by monolayer adsorption. The theoretical maximum adsorption capacity is 96.12 mg/g at 30 °C.

Table 2. Langmuir model and Freundlich model parameters**.**

Langmuir Model				Freundlich Model		
q_{max}	K_L	R_L	R^2	k_F	n	R^2
96.12	0.109	0.096	0.995	12.77	1.75	0.881

Kinetic study

The kinetic studies and the modeling of the experimental data are presented in Figure 10 and certain parameters are listed in Table 3 for models, it is verified that both models fit the experimental data well. Correlation parameters for the adsorption kinetics in the two models are shown in Table 3. As shown, the CIP adsorption on the adsorbent fits well with the pseudo-second-order kinetic model (R^2 = 0.992). This fit implies that the adsorption process occurs through chemical adsorption involving valence forces or electron exchange between CIP and the biosorbent, while the pseudo-first-order model assumes the occurrence of adsorption through physisorption.

Table 3. Obtained parameters of kinetics models for adsorption on MMC

Pseudo-first-order				Pseudo-second-order			
k_1	$q_{e.cal}$	$q_{e.exp}$	R^2	k_2	$q_{e.cal}$	$q_{e.exp}$	R^2
0.0897	4.74	9.712	0.949	0.0063	11.231	9.712	0.992

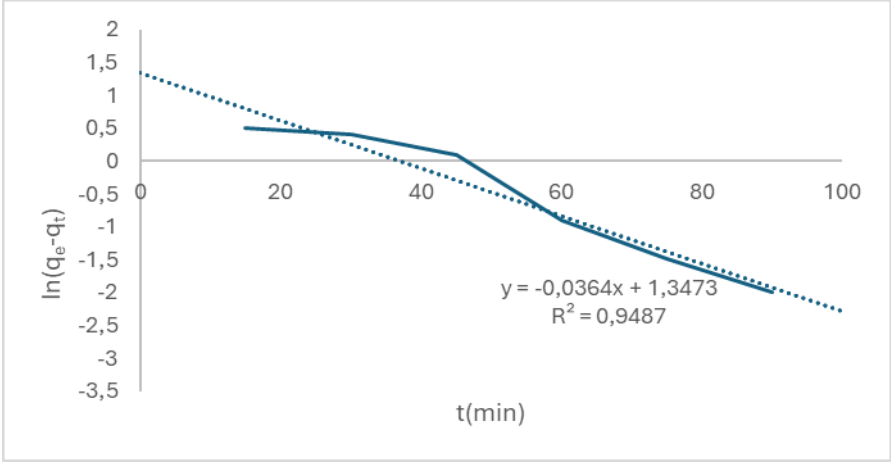

Figure 10(a). The analysis of determination of PFO of CIP adsorption onto MMC

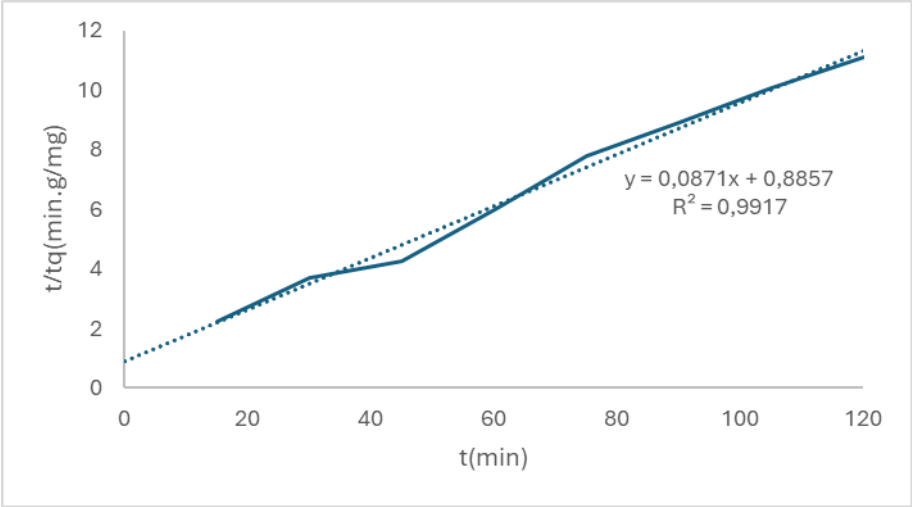

Figure 10(b). The analysis of determination of PSO of CIP adsorption onto MMC

The pseudo-second-order kinetic model, which best fits the experimental data in this study, had the highest correlation coefficient. A preliminary comparison in terms of adsorption rate (q_e) between the calculated and experimental values can be made to prove the best agreement, since the values calculated by the pseudo-second-order kinetic model are closer to the experimentally obtained ones. Such results demonstrate chemisorption reactions of adsorption of CIP molecules onto MMC (Pan, et al., 2011; Mohammed, Al-Musawi, Kareem, Zarrabi, & Al-Ma'abreh, 2020).

Adsorption thermodynamics

Results of thermodynamic parameters, which depend on the calculation of the temperature study, affect the nature of the adsorption process between adsorbent and adsorbate, be it physical or chemical adsorption (Zhang, et al., 2011; Erşan, Bağda, & Bağda 2013). The thermodynamic parameters are listed in Table 4. The negative values of ΔG° indicated that the adsorption performance of CIP on the MMC was feasible and spontaneous. Furthermore, the absolute values of ΔG° decreased with increasing temperature, indicating that the presence of a low-temperature energy barrier in adsorption and high-temperature adsorption was favorable (Balarak, Mahdavi, Bazrafshan, & Mahvi, 2016). The positive values of ΔH° confirmed the endothermic nature of the adsorption process, while the positive values of ΔS° indicated that the randomness at the solid-solution interface increased during the adsorption process (Balarak, & Azarpira, 2016).

Table 4. Thermodynamics parameters for CIP adsorption by MMC

T (K)	ΔG° (kJ/mol)	ΔH°(kJ/mol)	ΔS° (J/mol/K)
288	-3.37		
303	-4.84	3.07	0.03
323	-5.63		

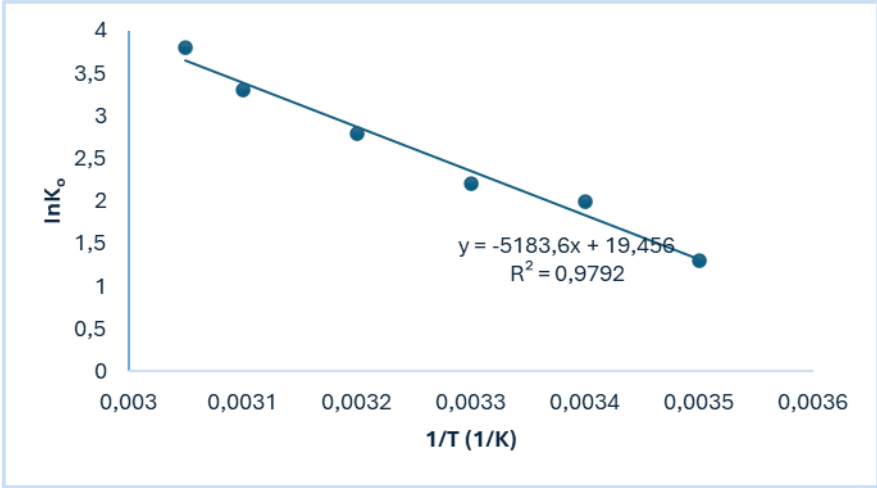

Figure 11. Graph of ln K vs. 1/T for the estimation of thermodynamic parameters of biosorption of CIP by MMC

Comparison with other adsorbents

Table 5 shows the determined maximum adsorption capacities for CIP using the current adsorbent and other materials tested in previous studies. Based on these results, the MMC used in the present study showed a high adsorption capacity for removing CIP molecules from aqueous solution compared to other adsorbents.

Table 5. shows the adsorption capacities of CIP on various sorbents

Adsorbent	Maximum adsorption capacity (mg/g)	Reference
Fe-pillared clays	122.1	(Roca Jalil, Baschini, & Sapag, 2017)
Magnetic activated carbon/chitosan	90	(Danalıoğlu, Bayazit, Kuyumcu, & Salam, 2017)
Cupric oxide nanoparticles	73.86	(Ahmadi, Banach, Mostafapour, & Balarak, 2017)
Magnetic mesoporous	98.3	(Shi, Fan, & Huang, 2013)
ZnO nanoparticles	8.3	(Dhiman, & Sharma, 2019)
Magnetic chitosan-grafted GO	282.9	(Wang, et al., 2016)
Current study	96.12	

CONCLUSION

The removal of the antibiotic ciprofloxacin (CIP) from aqueous solutions was thoroughly investigated in the current study using *Moringa oleifera* pods magnetized with magnetic iron (III) oxide (Fe_3O_4) nanoparticles. First, the used adsorbent was synthesized by the co-precipitation method. The characterization techniques like Fourier transform infrared spectrometry, thermogravimetric analyser and scanning electron microscope potential were used to identify different functional groups responsible for the adsorption, thermal stability and morphology of the nanoparticles. The Fourier transform infrared spectrometry confirmed different functional groups such as amine/amide, carbonyl, hydroxyl, carboxyl and iron oxide on modified magnetic iron oxide nanoparticles, which could be responsible for the selective recovery of ciprofloxacin. The scanning electron

microscope revealed a porous morphology with different pore sizes, which could be responsible for the retention of ciprofloxacin. The study also showed that the synthesized magnetic *moringa* composite (MMC) had excellent morphological properties, super paramagnetic value and brilliant active groups. The thermodynamic study showed that the ciprofloxacin adsorption was favorable, spontaneous, and endothermic. The results showed that the Langmuir isotherm and pseudo-second-order kinetic models were the best to describe the experimental isotherm and kinetic data of ciprofloxacin adsorption onto magnetic *moringa* composite.

ACKNOWLEDGEMENTS

The authors thank the Department of Chemistry Vaal University of Technology, Vanderbiljpark, South Africa for funding this work and the support

CONFLICT OF INTEREST

The authors declare that there is no conflict of interests regarding the publication of this article.

REFERENCES

Ahmadi, S., Banach, A., Mostafapour, F.K., & Balarak, D. (2017). Study survey of cupric oxide nanoparticles in removal efficiency of ciprofloxacin antibiotic from aqueous solution: Adsorption isotherm study. *Desal Water Treat*, 89, 297-303.

Araujo, C.S.T., Alves, V.N., Rezend, H.C., Almeida, I.L.S., de Assuncao, R.M.N., Tarley, C.R.T., Segatelli, M.G., & Coelho, N.M.M. (2010). Characterization and use of *Moringa oleifera* seeds as biosorbent for removing metal ions from aqueous effluents. *Wat Sci Tech*, *62*(9), 2198-2203.

Avella, A.C., Delgado, L.F., Görner, T., Albasi, C., Galmiche, M., & De Donato, P. (2010). Effect of cytostatic drug presence on extracellular polymeric substances formation in municipal wastewater treated by membrane bioreactor. *Bioresource technology*, *101*(2), 518-526.

Balarak, D., & Azarpira, H. (2016). Rice husk as a biosorbent for antibiotic metronidazole removal: Isotherm studies and model validation. *International Journal of Chem Tech Research*, *9*(7), 566-573.

Balarak, D., Mahdavi, Y., Bazrafshan, E., & Mahvi, A.H. (2016). Kinetic, isotherms and thermodynamic modeling for adsorption of acid blue 92 from aqueous solution by modified *Azolla filicoloides*. *Fresenius Environmental Bulletin*, *25*(5), 1322-1331.

Carabineiro, S.A.C., Thavorn-Amornsri, T., Pereira, M.F.R., Serp, P., & Figueiredo, J.L. (2012). Comparison between activated carbon, carbon xerogel and carbon nanotubes for the adsorption of the antibiotic ciprofloxacin. *Catal Today*, *186*, 29-34.

Celik, M.S., & Ozdemir, O. (2018). Hetero coagulation of hydrophobized particulates by ionic surfactants. *Physicochem Probl Miner Process*, *54*(1), 124-130.

Danalıoğlu, S.T., Bayazit, Ş.S., Kuyumcu, Ö.K., & Salam, M.A. (2017). Efficient removal of antibiotics by a novel magnetic adsorbent: Magnetic activated carbon/chitosan (MACC) nanocomposite. *J Mol Liq*, *240*, 589-596.

Dhiman, N., & Sharma, N. (2019). Batch adsorption studies on the removal of ciprofloxacin hydrochloride from aqueous solution using ZnO nanoparticles and groundnut (Arachis hypogaea) shell powder: a comparison. *Indian Chemical Engineer*, *61*(1), 67-76.

Ehrampoush, M.H., Miria, M. Salmani, M.H., & Mahvi, A.H. (2015). Cadmium removal from aqueous solution by green synthesis iron oxide nanoparticles with tangerine peel extract. *J Environ Health Sci Eng*, *13*, 1-7.

Erşan, M., Bağda, E., & Bağda, E. (2013). Investigation of kinetic and thermodynamic characteristics of removal of tetracycline with sponge like, tannin based cryogels. *Colloids Surf B Biointerfaces*, *104*, 75-82.

Gleick, P.H. (2003). Global freshwater resources: soft-path solutions for the 21st century. *Science*, *302*(5650), 1524-1528.

Gu, C., & Karthikeyan, K.G. (2005). Sorption of the antimicrobial ciprofloxacin to aluminium and iron hydrous oxides. *Environ Sci Technol*, *39*(23), 9166-9173.

Guerra, D. L., Lemos, V. P., Airoldi, C., & Angélica, R. S. (2006). Influence of the acid activation of pillared smectites from Amazon (Brazil) in adsorption process with butylamine. *Polyhedron*, *25*(15), 2880-2890.

Kakavandi, B., Esrafily, A., Mohseni-Bandpi, A., Jafari, A.J., & Kalantary, R.R. (2013). Magnetic Fe_3O_4@C nanoparticles as adsorbents for removal of amoxicillin from aqueous solution. *Water Sci. Technol*, *69*(1), 147-155.

Kandpal, N.D., Sah, N., Loshali, R., Joshi, R., & Prasad, J. (2014). Co-Precipitation Method of Synthesis and Characterization of Iron Oxide Nanoparticles. *Journal of Scientific & Industrial Research*, *73*(2), 87-90.

Li, Z., Hong, H., Liao, L., Ackley, C.J., Schulz, L.A., MacDonald, R.A., Mihelich, A.L., & Emard, S.M. (2011). A mechanistic study of ciprofloxacin removal by kaolinite. *Colloid Surf B*, *88*, 339-344.

Machado, M. O., Lazarin, A. M., & Airoldi, C. (2006). Thermodynamic features associated with intercalation of some n-alkylmonoamines into barium phosphate. *The Journal of Chemical Thermodynamics*, *38*(2), 130-135.

Mohammed, A.A., Al-Musawi, T.J., Kareem, S.L., Zarrabi, M., & Al-Ma'abreh, A.M. (2020). Simultaneous adsorption of tetracycline, amoxicillin, and ciprofloxacin by pistachio shell powder coated with zinc oxide nanoparticles. *Arab J Chem*, *13*(3), 4629-4643.

Mushtaq, N., Singh, D.V., Bhat, R.A., Dervash, M.A., & Hameed, O. (2020). Freshwater Contamination: Sources and Hazards to Aquatic Biota. *Fresh Water Pollut Dyn Remediat*, 27-50.

Nasseh, N., Al-Musawi, T.J., Miri, M.R., Rodriguez-Couto, S., & Hossein Panahi, A. (2020). A comprehensive study on the application of $FeNi_3$@SiO_2@ZnO magnetic nanocomposites as a novel photocatalyst for degradation of tamoxifen in the presence of simulated sunlight. *Environ Pollut*, *261*, 114127.

Oliveira, L.C.A., Rios, R.V.R.A., Fabris, J.D., Sapag, K., Garg, V.K., & Lago, R.M. (2003). Clay-iron oxide magnetic composites for the adsorption of contaminants in water. *Appl Clay Sci*, *22*(4), 169-177.

Pan, J., Yao, H., Guan, W., Ou, H., Huo, P., Wang, X., Zou, X., & Li, C. (2011). Selective adsorption of 2,6-dichlorophenol by surface imprinted polymers using polyaniline/silica gel composites as functional support: Equilibrium, kinetics, thermodynamics modelling. *Chem Eng J*, *172*(2), 847-855.

Reynaud, F., Tsapis, N., Deyme, M., Vasconcelos, T.G., Gueutin, C., Guterres, S.S., Pohlmann, A.R., & Fattal, E. (2011). Spray-dried chitosan–metal microparticles for ciprofloxacin adsorption: kinetic and equilibrium studies. *Soft Matter*, *7*, 7304-7312.

Roca Jalil, M. E., Baschini, M., & Sapag, K. (2017). Removal of ciprofloxacin from aqueous solutions using pillared clays. *Materials*, *10*(12), 1345.

Shi, S., Fan, Y., & Huang, Y. (2013). Facile low temperature hydrothermal synthesis of magnetic mesoporous carbon nanocomposite for adsorption removal of ciprofloxacin antibiotics. *Ind Eng Chem Res*, *52*(7), 2604-2612.

Sun, S.P., Hatton, T.A., & Chung, T.S. (2011). Hyperbranched polyethyleneimine induced cross-linking of polyamide-imide nanofiltration hollow fiber membranes for effective removal of ciprofloxacin. *Environ Sci Technol*, *45*(9), 4003-4009.

Tavengwa, N. T., Cukrowska, E., & Chimuka, L. (2016). Application of raw and biochared Moringa oleifera seed powder for the removal of nitrobenzene from aqueous solutions. *Desalination and Water Treatment*, *57*(53), 25551-25560.

Van Doorslaer, X., Demeestere, K., Heynderickx, P.M., Van Langenhove, H., & Dewulf, J. (2011). UV-A and UV-C induced photolytic and photocatalytic degradation of aqueous ciprofloxacin

and moxifloxacin: reaction kinetics and role of adsorption. *Applied Catalysis B: Environmental*, *101*(3-4), 540-547.

Wang, C.J., Li, Z., & Jiang, W.T. (2011). Adsorption of ciprofloxacin on 2:1 dioctahedral clay minerals. *Appl Clay Sci*, *53*, 723-728.

Wang, F., Yang, B., Wang, H., Song, Q., Tan, F., & Cao, Y. (2016). Removal of ciprofloxacin from aqueous solution by a magnetic chitosan grafted graphene oxide composite. *J Mol Liq*, *222*, 188-194.

World Health Organization. (2017). *Guidelines for Drinking-water Quality*, 91.

Witte, B.D., Langenhove, H.V., Demeestere, K., Saerens, K., Wispelaere, P.D., & Dewulf, J. (2010). Ciprofloxacin ozonation in hospital wastewater treatment plant effluent: Effect of pH and H_2O_2. *Chemosphere*, *78*(9), 1142-1147.

Yahya, M.S., Oturan, N., El-Kacemi, K., El-Karbane, M., Aravindakumar, C.T., & Oturan, M.A. (2014). Oxidative degradation study on antimicrobial agent ciprofloxacin by electro-fenton process: kinetics and oxidation products. *Chemosphere*, *117*, 447-454.

Yıldız, N., Erol, M., Aktas, Z., & Çalımlı, A. (2004). Adsorption of Aromatic Hydrocarbons on BTEA–bentonites. *Adsorption Science & Technology*, *22*(2), 145-154.

Zhang, C. L., Qiao, G. L., Zhao, F., & Wang, Y. (2011). Thermodynamic and kinetic parameters of ciprofloxacin adsorption onto modified coal fly ash from aqueous solution. *Journal of Molecular Liquids*, *163*(1), 53-56.

Zhang, L., Song, X., Liu, X., Yang, L., Pan, F., & Lv, J. (2011). Studies on the removal of tetracycline by multi-walled carbon nanotubes. *Chem Eng J*, *178*, 26-33.